




**Multi-GeV wakefield acceleration in a plasma-modulated plasma accelerator**J. J. van de Wetering <sup>1,\*</sup>, S. M. Hooker <sup>1</sup> and R. Walczak <sup>1,2</sup><sup>1</sup>*John Adams Institute for Accelerator Science and Department of Physics, University of Oxford, Denys Wilkinson Building, Keble Road, Oxford OX1 3RH, United Kingdom*<sup>2</sup>*Somerville College, Woodstock Road, Oxford OX2 6HD, United Kingdom*

(Received 2 November 2023; accepted 11 January 2024; published 6 February 2024)

We investigate the accelerator stage of a plasma-modulated plasma accelerator (P-MoPA) [Jakobsson *et al.*, *Phys. Rev. Lett.* **127**, 184801 (2021)] using both the paraxial wave equation and particle-in-cell (PIC) simulations. We show that adjusting the laser and plasma parameters of the modulator stage of a P-MoPA allows the temporal profile of pulses within the pulse train to be controlled, which in turn allows the wake amplitude in the accelerator stage to be as much as 72% larger than that generated by a plasma beat-wave accelerator with the same total drive laser energy. Our analysis shows that Rosenbluth-Liu detuning is unimportant in a P-MoPA if the number of pulses in the train is less than  $\sim 30$ , and that this detuning is also partially counteracted by increased red-shifting, and hence increased pulse spacing, towards the back of the train. An analysis of transverse mode oscillations of the driving pulse train is found to be in good agreement with 2D (Cartesian) PIC simulations. PIC simulations demonstrating energy gains of  $\sim 1.5$  GeV ( $\sim 2.5$  GeV) for drive pulse energies of 2.4 J (5.0 J) are presented. Our results suggest that P-MoPAs driven by few-joule, picosecond pulses, such as those provided by high-repetition-rate thin-disk lasers, could accelerate electron bunches to multi-GeV energies at pulse repetition rates in the kilohertz range.

DOI: [10.1103/PhysRevE.109.025206](https://doi.org/10.1103/PhysRevE.109.025206)**I. INTRODUCTION**

Proposed in 1979 by Tajima and Dawson, laser wakefield accelerators (LWFAs) [1] can outperform the accelerating gradients of conventional radio-frequency cavities by up to three orders of magnitude. In a LWFA, an ultrashort laser pulse excites a plasma wave wake by pushing free electrons via the ponderomotive force while the heavier ions remain approximately stationary. The separation of electrons and ions generates large electric fields, which propagate with a phase velocity set by the group velocity of the laser pulse, and are therefore suitable for accelerating relativistic charged particles.

For a laser pulse to efficiently excite a plasma wave, its duration must be less than half the plasma period  $T_p = 2\pi/\omega_p$ , which is in the 100 fs range for plasma densities of interest. Because sufficiently short joule-scale pulses were not yet feasible, Tajima and Dawson proposed the plasma beatwave accelerator (PBWA) [1]. In this configuration, two long copropagating pumps with a carrier frequency mismatch approximately equal to the plasma frequency  $\Delta\omega = \omega_1 - \omega_2 \approx \omega_p$  interfere to form a train of short pulses via beat-wave modulation. The resulting cosine-squared intensity

modulation corresponds to a train of pulses spaced by  $T_p$  that can resonantly excite a plasma wave [1–5]. More generally, we will refer to resonant wakefield excitation with trains of uniformly or nonuniformly spaced pulses as multipulse-LWFA (MP-LWFA) [6].

The great majority of recent LWFA experiments have instead used single high intensity ultrashort ( $< 100$  fs) laser pulses from Ti:sapphire laser systems enabled by the development of chirped pulse amplification [7]. At high pulse energies ( $> 1$  J), these laser systems are restricted to low ( $\sim 0.1$ – $10$  Hz) repetition rates [8] and have poor ( $< 0.1\%$ ) electrical-to-optical energy efficiencies [9]. These limitations reduce the number of applications for which these LWFAs offer an advantage over conventional, radio-frequency particle accelerators.

To tackle these issues, a scheme was recently proposed [10] which we have dubbed the plasma-modulated plasma accelerator (P-MoPA). This approach aims to drive high repetition rate and multi-GeV plasma accelerators with thin-disk lasers which are both efficient and can provide multijoule laser pulses at kHz repetition rates [11–13]. These laser systems cannot be used to drive LWFAs directly since the duration of the pulses they provide is too long:  $\tau \gtrsim 1$  ps for joule-scale pulses [14–16]. To overcome this limitation, in a P-MoPA the drive pulse is spectrally broadened by adding multiple sidebands spaced by the plasma frequency using a modulator stage. This is followed by a dispersive optical system that removes the spectral phase exhibited by the sidebands to generate a train of short pulses that can be used to resonantly excite a wakefield in an accelerator stage. This scheme is related to the PBWA since in both schemes the wakefield is

\*johannes.vandewetering@physics.ox.ac.uk

resonantly excited by a train of laser pulses. However, the P-MoPA differs from the PBWA in two important ways. First, in a P-MoPA only a single input driver frequency is required to generate the pulse train. This avoids the requirement for two driving systems that differ in output frequency by precisely the plasma frequency. Second, the temporal profile of the pulse trains generated in a P-MoPA can be controlled and can excite the wakefield more efficiently than the cosine-squared profile pulse trains generated in a PBWA.

In this paper, we study the performance of multi-GeV MP-LWFAs driven by P-MoPA pulse trains; it builds on our earlier work that established the range of parameters for which operation of the modulator stage was stable [17]. We derive a full 3D analytic theory of the pulse train and wakefield evolution in long plasma channels and compare the results with 2D (Cartesian) PIC simulations using WARPX [18], using a grid resolving the laser wavelength  $\lambda_L$  by  $\Delta z = \lambda_L/44$  longitudinally and  $\Delta x = \lambda_L/2.5$  transversally. We use these results to optimize the performance of P-MoPAs, which are set by both the dynamics of the accelerator stage as well as the previously derived constraints on the modulator stage [17]. We explore the key differences between the pulse trains formed by P-MoPA and PBWA. We find that a beneficial feature of the P-MoPA scheme is the ability to control the longitudinal profile of the pulses in the train independent of their pulse spacing; this allows for more resilient pulse trains and more efficient wake excitation than PBWA, as well as offering a degree of control over the onset of depletion effects.

## II. SCALING LAWS

Since the P-MoPA accelerator stage necessarily operates in the (quasi)linear regime, we expect the energy gain scaling laws for a P-MoPA to be similar to those of the single pulse linear regime [19]. In this section, we outline these scaling laws, taking into account the effect of finite spot size effects on the laser group velocity.

To extend the acceleration length beyond the Rayleigh range, the pulse train is guided in a preformed plasma channel. A parabolic plasma channel matched to a Gaussian pulse of spot size  $w_0$  has a transverse electron density profile given by [20–22]

$$n_0(r) = n_{00} + \Delta n(r/w_0)^2, \quad (1)$$

where  $n_{00}$  is the on-axis plasma density and  $\Delta n = (\pi r_e w_0^2)^{-1}$  is the channel depth parameter with  $r_e$  being the classical electron radius. The corresponding group velocity of a Gaussian pulse propagating in such a matched channel, including finite spot size effects, is given by [22]

$$\frac{v_g}{c} = 1 - \frac{\omega_{p0}^2}{2\omega_L^2} - \frac{2c^2}{\omega_L^2 w_0^2}, \quad (2)$$

where  $\omega_{p0} = \omega_p(r=0)$  indicates the on-axis plasma frequency. We note that the contributions to the reduction in  $v_g$  of the finite spot size and plasma density are equal when  $w_0 = 2c/\omega_{p0}$ , which for an on-axis plasma density of  $n_{00} = 1.0 \times 10^{17} \text{ cm}^{-3}$  corresponds to  $w_0 = 34 \mu\text{m}$ .

From Eq. (2), the dephasing length, defined as the propagation distance over which an electron propagating at  $c$  slips

relative to the wakefield by one-quarter plasma wavelength  $\sim \lambda_{p0}/4$  (assuming no channel effects on wake structure), is

$$L_d = \frac{\lambda_{p0}}{4} \left( \frac{\omega_{p0}^2}{2\omega_L^2} + \frac{2c^2}{\omega_L^2 w_0^2} \right)^{-1}. \quad (3)$$

Note that a method has been proposed [23] which allows MP-LWFAs to accelerate beyond the dephasing length by introducing a short region of higher plasma density, which lets the accelerated electron bunch to rephase into the next accelerating bucket back at the resonant density without deceleration.

Integrating the equations of motion for a relativistic particle moving in a sinusoidal wakefield gives the energy gain  $\Delta W_e$  before the onset of dephasing as

$$\frac{\Delta W_e}{m_e c^2} \approx \frac{2}{\pi} \frac{e E_{\max} L_d}{m_e c^2} = 2 \frac{E_{\max}}{E_{\text{wb}}} \frac{\omega_L^2}{\omega_{p0}^2 + 4c^2/w_0^2}, \quad (4)$$

where  $E_{\max}$  is the peak accelerating field and  $E_{\text{wb}} = m_e \omega_{p0} c / e$  is the cold wave-breaking field. This shows that for a given spot size, the maximum energy gain cannot be increased indefinitely by reducing the plasma density, as the dephasing length becomes dominated by finite spot size effects. This is a well-known effect in LWFA [24], where the prescription is to scale the spot size with the plasma density such that

$$w_0 \gtrsim \frac{2c}{\omega_{p0}} = \frac{\lambda_{p0}}{\pi}. \quad (5)$$

On top of preventing an excessive reduction in group velocity, scaling the spot size this way also prevents the wakefield from becoming largely radial [24,25]. As the required spot size increases with the plasma wavelength, the total laser energy must necessarily increase. The total energy of the pulse train  $W_{\text{drive}}$  required to excite a given accelerating field relative to the wave-breaking field  $E_{\max}/E_{\text{wb}}$  scales with the volume enclosed by the spot size and the plasma length, i.e.,  $W_{\text{drive}} \sim w_0^2 \lambda_{p0} \sim \lambda_{p0}^3$ . This grows faster with the plasma wavelength than the electron energy gain  $\Delta W_e \sim \lambda_{p0}^2$  and the maximum bunch charge  $Q_e \sim n_{00} w_0^2 \lambda_{p0} \sim \lambda_{p0}$ , but the overall laser-to-bunch energy efficiency  $Q_e \Delta W_e / e W_{\text{drive}}$  has no plasma density scaling. These scaling laws, which we have derived for pulse trains in the linear regime, are identical to that of a linear single pulse LWFA [19].

Another limit to acceleration is pump depletion. Similar to the dephasing length, the depletion length will also be reduced by finite spot-size effects. This is due to the extra pulse energy spent exciting the aforementioned transverse wakefield for pulses with spot sizes comparable to the plasma wavelength. The depletion length can be estimated by comparing the laser energy with the energy contained within the linear wakefield and its transverse counterpart spanning the depletion length  $L_{\text{pd}}$ . Assuming that the pulse train is resonantly spaced and is comprised of individual linearly polarized Gaussian pulses of the form  $a_m^2 = a_{0,m}^2 \exp(-(\xi - \xi_{0,m})^2 / L^2)$ , where  $m = 1, 2, \dots, N$ , and that each pulse is short (i.e.,  $L \ll \lambda_{p0}$ ) so each pulse increases the normalized wake amplitude [26] by  $\sqrt{\pi/2} a_{0,m}^2 k_{p0} L / 4$ , the pump depletion length is given by

$$L_{\text{pd}} = \left( \frac{\pi E_{\max}}{8 E_{\text{wb}}} \right)^{-1} L_d. \quad (6)$$

Note that this derivation is identical to that for single pulse LWFA. This expression shows that the depletion length is always larger than the dephasing length in the linear wakefield regime, which is also true for single pulse LWFA [19]. To make efficient use of the available laser energy, we would ideally want the pump depletion length to be larger but similar to the dephasing length. As this is not feasible, the P-MoPA accelerator stage should at least be operated in the quasilinear regime, while avoiding nonlinear detuning effects associated with the large amplitude wake, which will be discussed later. We also note that this treatment of the depletion length is too simplistic for pulse trains since, as we will show later, it does not capture the different rates at which each of the pulses deplete.

### III. CHANNEL EFFECTS ON ENERGY GAIN

Driving the accelerator within a preformed plasma channel causes the laser to remain focused well beyond the Rayleigh range. However, the transverse variation of plasma density within the channel leads to a concomitant variation of the plasma frequency that can also influence the structure of the excited wakefield and hence the energy gain of an injected electron bunch.

It is well-known for single-pulse LWFA that plasma channels can strongly influence wakefield structure via the curvature of wake phase fronts [27]. For example, shallow parabolic channels matched to the spot size  $w_0$ , i.e.,  $\frac{1}{2}k_{p0}^2 w_0^2 \gg 1$ , increase the overlap between the accelerating and focusing regions of the wakefield by up to a factor of 2 at sufficient distances behind the laser pulse. This can be beneficial for acceleration, as it can increase the dephasing length by a factor of up to 2 without sacrificing much accelerating gradient. However, deep matched parabolic channels, i.e., those for which  $\frac{1}{2}k_{p0}^2 w_0^2 < 1$ , yield a rapid conversion of axial field into radial field with distance behind the drive pulse, meaning that LWFA is only possible in the first few buckets behind the drive pulse. This quick conversion of axial field into radial field readily outpaces other known wakefield decay mechanisms, such as the ion motion modulational instability [28], which only becomes relevant on the ion plasma frequency timescale, corresponding to about 40 plasma wavelengths for hydrogen. Therefore, the transverse profile of the plasma channel is the dominant effect determining damping of the accelerating wakefield, and hence the useful number of pulses in the train.

When using a single pulse driver, the channel effect on wake structure only needs to be considered for one plasma wavelength behind the driver. However, for a pulse train comprised of  $N$  pulses, the channel influence on wake structure is relevant over  $N$  plasma wavelengths. The depth of a parabolic channel will therefore determine the maximum useful number of pulses used in a MP-LWFA, as the axial wakefield contribution of the first pulse in a train will disappear by the time the  $N$ th pulse passes. There are two ways to allow for longer trains. The first way is to operate well in the shallow channel limit  $\frac{1}{2}k_{p0}^2 w_0^2 \gg N$ . However, this forces the required matched spot size to become large at low plasma densities and large pulse train lengths (e.g.,  $w_0 \gg 75 \mu\text{m}$  at  $n_{00} = 1.0 \times 10^{17} \text{cm}^{-3}$ ,  $N = 10$ ), bringing the required laser energy to drive the wakefield in the quasi-linear regime to the 10-joule

scale for a 1030 nm laser wavelength. The other solution is to use square-profile channels, which have a much weaker effect on the wakefield structure. Fortunately, the transverse density profiles of conditioned hydrodynamic optical-field-ionized (CHOFI) plasma waveguides are closer to square than parabolic in shape [29–31], which makes them well-suited to driving P-MoPAs.

An example PIC simulation of the wake structure driven by a P-MoPA pulse train is presented in Fig. 1, where the pulse train is guided in a quasi-square channel of the form

$$\frac{n_0(r) - n_{00}}{\Delta n} = \begin{cases} (r/R)^{10} & r < 1.2R \\ (1.2)^{10} & 1.2R \leq r < 1.2R + d \\ (1.2)^{10} \left(1 - \frac{r-1.2R-d}{d}\right) & 1.2R + d \leq r < 1.2R + 2d \\ 0 & \text{otherwise,} \end{cases} \quad (7)$$

where  $R$ ,  $\Delta n = (\pi r_e R^2)^{-1}$ , and  $d = 10 \mu\text{m}$  are the channel wall radius, depth, and thickness parameters, respectively. Resonant excitation of a large amplitude  $\sim 50\%$  wakefield on axis is evident. Also apparent is a large amplitude wakefield on the inner wall of the channel. This is due to the steep plasma density gradient

$$\frac{d \ln n_0}{dr} > k_p, \quad (8)$$

which is characteristic of plasma channels at these spot sizes and low  $\sim 10^{17} \text{cm}^{-3}$  on-axis densities. The wake amplitude in this region continues to grow even after the laser driver has already passed due to the aforementioned conversion of the wakefield from the longitudinal to transverse component [27]. This accumulated wall-boundary wake can eventually exceed the on-axis wake amplitude, suggesting that large-amplitude wake fields driven by pulse trains in plasma channels would undergo transverse wave-breaking effects before longitudinal wave breaking.

### IV. P-MOPA PULSE SHAPING

The plasma modulator offers a degree of control of the temporal profile of the pulses in the pulse train, allowing for further optimization of the accelerator stage. The pulse train formed after compression is comprised of pulses evenly spaced by the modulator plasma period with pulse heights and durations determined by the amount of spectral modulation introduced by the modulator stage. The additional bandwidth of the spectrally modulated drive pulse enables a P-MoPA to form pulses substantially shorter than their separation, unlike the cosine-squared pulses created with the beat-wave method. This allows larger wake amplitudes to be driven in a P-MoPA with the same drive pulse energy.

According to 3D spectral modulation theory [17], assuming that the spectral modulation remains primarily in the fundamental channel mode, the pulse trains formed using the “ideal compressor” described by Jakobsson *et al.* [10], with a seed wake of the form  $\delta n(r, \xi) = \delta n_s \cos(k_{p0} \xi) \exp(-2r^2/w_0^2)$ , will have the following

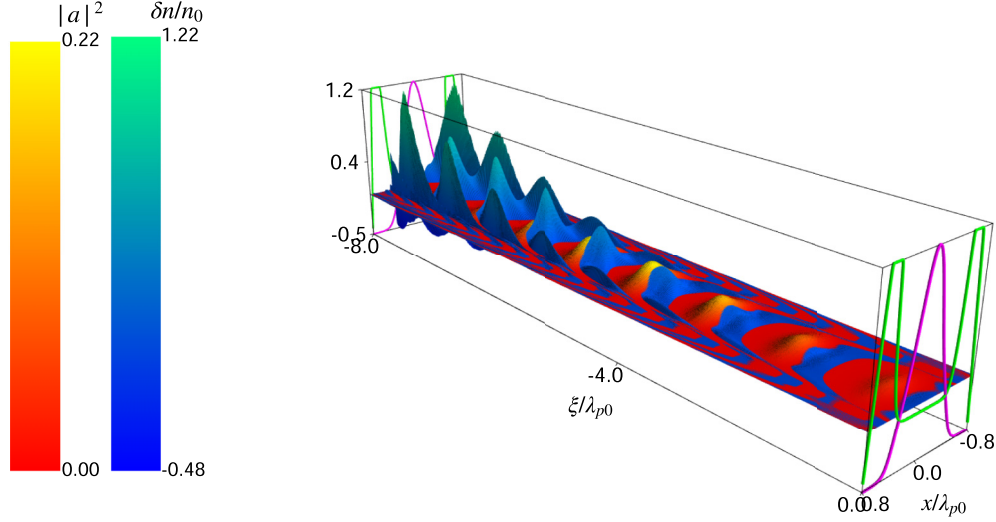


FIG. 1. Snapshot at  $z = 2.1$  mm of the relative plasma density perturbation  $\delta n/n_0$  (blue-green) resonantly excited by a P-MoPA pulse train with normalized intensity  $|a|^2$  (red-yellow). The transverse electron density profile of the channel, corresponding to Eq. (7) (green), and the longitudinally averaged transverse intensity profile (purple) of the drive pulses are shown on the end panel of the plot. Results are from a 2D simulation using the PIC code WARPX [18] with  $W_{\text{drive}} = 1.2$  J,  $\tau_{\text{drive}} = 1$  ps,  $\lambda_L = 1030$  nm,  $R = 30$   $\mu\text{m}$ ,  $w_0 = 30$   $\mu\text{m}$ ,  $n_{00} = 2.5 \times 10^{17}$   $\text{cm}^{-3}$ , and modulator parameter  $\beta = 1.2$  as defined in Eq. (9) (note that for 2D Cartesian geometry, the laser energy  $W_{\text{drive}}$  determines the initial  $a_0$  of the laser pulse at focus as if it were 3D assuming a cylindrically symmetric Gaussian transverse profile).

temporal amplitude envelope:

$$f_{\text{acc}}(\xi; \beta) = f_{\text{mod}}(\xi) \left( J_0(\beta) + 2 \sum_{n=1}^{\infty} J_n(\beta) \cos(nk_p \xi) \right),$$

$$\beta = \frac{2\Omega_s L_{\text{mod}}}{v_{g,\text{mod}}}, \quad (9)$$

where  $\xi = z - ct$  is the longitudinal comoving coordinate,  $0 \leq f_{\text{mod}}(\xi) \leq 1$  is the input temporal amplitude envelope,  $L_{\text{mod}}$  is the modulator length,  $v_{g,\text{mod}}$  is laser group velocity, and  $\Omega_s = (\omega_{p0}^2/8\omega_L)(\delta n_s/n_{00})$  is the rate of spectral modulation of a Gaussian pulse co-propagating with a seed wake of on-axis amplitude  $\delta n_s$  in a parabolic channel [17]. The modulator parameter  $\beta$  determines the effective number of sidebands generated in the drive pulse spectrum and controls the temporal profile of the pulse train produced by the plasma modulator (while obeying the modulator stability condition outlined in Ref. [17]). Figure 2 shows how the temporal intensity profiles of the pulses within the train, their full-length at half maximum duration, and their contrast, varies with  $\beta$ . It can be seen that adjusting the parameter  $\beta$  allows the duration and contrast of the pulses within the train to be controlled.

The peak intensity occurs at  $\beta = j_{0,1} \approx 2.405$ , where  $j_{m,n}$  indicates the  $n$ th nonzero root of the Bessel function  $J_m(x)$ . This can be shown by evaluating the temporal envelope at the pulse center using well-known identities for Neumann series of Bessel functions [32,33]

$$\frac{f_{\text{acc}}(0; \beta)}{f_{\text{mod}}(0)} = J_0(\beta) + 2 \sum_{n=1}^{\infty} J_n(\beta)$$

$$= 1 + \int_0^\beta J_0(s) ds, \quad (10)$$

which shows that its global maximum occurs at  $\beta = j_{0,1}$ , where it takes the value  $f_{\text{acc}} \approx 2.470 f_{\text{mod}}$ . As evident in Fig. 2, increasing  $\beta$  above this value leads to the formation of shorter pulses, but these have temporal wings, which wastes energy since they do not contribute to wake excitation. Thus

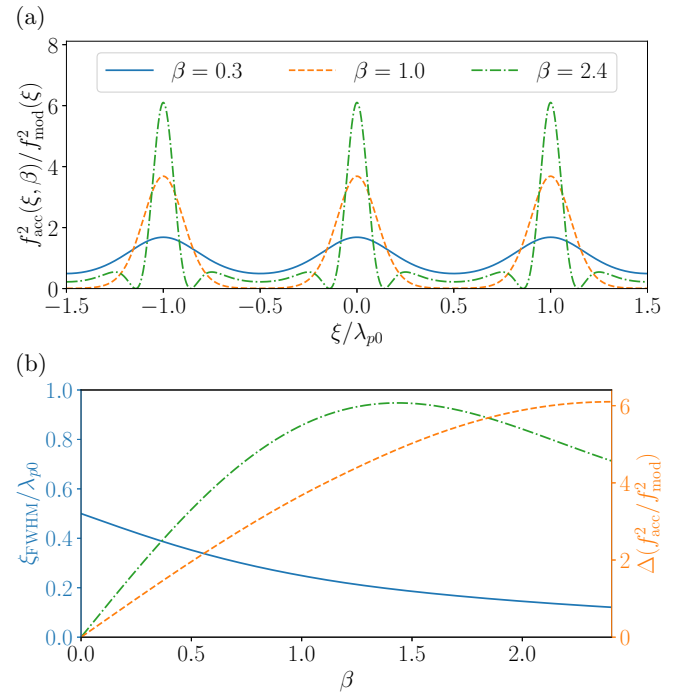


FIG. 2. (a) Pulse train temporal profiles for various values of the modulator parameter  $\beta$  and their respective FWHM durations (dashed). (b) FWHM duration (blue, solid), peak prominence (orange, dashed) and the wakefield amplitude according to 1D linear theory (green, dot-dashed, arb. units) as a function of  $\beta$ .



when optimizing the P-MoPA scheme, we only need to consider  $\beta \leq j_{0,1}$ .

The additional control that the parameter  $\beta$  provides enables more efficient wake excitation than is possible with PBWA. This is shown in Fig. 2(b), which shows that  $\beta$  in the range of 1.1–1.6 optimizes the wake amplitude according to linear wakefield theory [19]. We can also show in the linear regime that the ratio between the amplitude of the wake potential driven by a P-MoPA pulse train and an ideal beat-wave pulse train with a temporal intensity modulation of the form  $1 + \cos(k_{p0}\xi)$  containing the same laser energy is given by

$$\begin{aligned} \frac{\phi_{\text{P-MoPA}}}{\phi_{\text{PBWA}}} &= \frac{\int_{-\pi}^{\pi} [J_0(\beta) + 2 \sum_{n=1}^{\infty} J_n(\beta) \cos(ns)]^2 \cos(s) ds}{\int_{-\pi}^{\pi} [1 + \cos(s)] \cos(s) ds} \\ &= 4 \sum_{n=0}^{\infty} J_n(\beta) J_{n+1}(\beta) \\ &= 2\beta [J_0^2(\beta) + J_1^2(\beta)]. \end{aligned} \quad (11)$$

This ratio is maximized for  $\beta \approx 1.43$ , at which value the wake amplitude in a P-MoPA is 72% larger than that driven by an ideal PBWA with the same total drive energy.

## V. THE ROSENBLUTH-LIU LIMIT

Resonant wakefield acceleration requires the driving pulses to be spaced by the plasma period. However, as the plasma wave amplitude increases beyond the linear regime, its wavelength increases due to relativistic effects. The consequent buildup of plasma wave phase difference relative to the laser pulse centroids sets a limit on the maximum wake amplitude achievable.

The saturation effect arising from this detuning was derived by Rosenbluth and Liu [2] in the context of plasma beat-wave excitation. In their derivation, two infinite-duration pumps with normalized vector potential amplitudes  $a_1$  and  $a_2$  interfere to form a cosine beat-wave pulse train resonant with the plasma, which results in the saturated wakefield amplitude scaling with the third root of the intensity of the beat-wave modulation:

$$\frac{E_{\text{sat}}}{E_{\text{wb}}} = \left( \frac{16a_1 a_2}{3} \right)^{1/3}. \quad (12)$$

P-MoPA pulse trains, which are also spaced uniformly by design, are thus expected to exhibit a similar limit. However, for a P-MoPA, an important difference is that the train will comprise a relatively small number of pulses.

According to 1D nonlinear plasma wave theory [19], the nonlinear correction to the plasma wavelength for a plasma wave of amplitude  $\phi_a = E_a/E_{\text{wb}}$  at nonrelativistic laser intensities in the  $\phi_a^2 \ll 1$  limit is given by

$$\begin{aligned} \lambda_p^{\text{NL}} &\approx \lambda_p (1 + 3\phi_a^2/16), \\ k_p^{\text{NL}} &\approx k_p (1 - 3\phi_a^2/16). \end{aligned} \quad (13)$$

Resonant excitation of the wakefield eventually saturates due to detuning caused by the progressive growth of the plasma wavelength. The comoving coordinate  $\xi_{\text{sat}}$  at which this

detuning occurs is approximately given by

$$\int_{\xi_{\text{sat}}}^{\infty} (k_p - k_p^{\text{NL}}) d\xi \approx \frac{\pi}{2}. \quad (14)$$

Since the pulse train in a P-MoPA pulse train corresponds to a sequence of short pulses spaced by  $T_p$ , within an envelope determined by the duration of the ps-duration drive pulse, most of its energy will be contained within only a few pulses close to its center. To account for this, we model the original pulse envelope as a temporally Gaussian pulse of the form

$$f_{\text{mod}}^2(\xi) = \exp\left(-\frac{\xi^2}{2\sigma^2}\right), \quad (15)$$

where  $\sigma = c\tau_{\text{drive}}/2\sqrt{2\ln 2}$ , with  $\tau_{\text{drive}}$  being the FWHM duration of the drive pulse. From linear theory, ignoring detuning, the wakefield potential amplitude  $\phi_a(\xi)$  excited by the pulse train is given by

$$\frac{\phi_a(\xi)}{\phi_{\text{max}}} = \frac{\int_{\xi}^{\infty} d\xi' f_{\text{acc}}^2(\xi')}{\int_{-\infty}^{\infty} d\xi' f_{\text{acc}}^2(\xi')} \approx \frac{1}{2} \operatorname{erfc}\left(\frac{\xi}{\sqrt{2}\sigma}\right), \quad (16)$$

where  $\phi_{\text{max}} = E_{\text{max}}/E_{\text{wb}}$  is the maximum wakefield amplitude resonantly excited by the pulse train. For the pulse train to efficiently drive a wakefield, resonant detuning must not occur before the majority of the pulses have already passed. If we demand that at least  $\sim 90\%$  of the pulse train energy passes before the full  $\pi/2$  detuning occurs, then combining Eqs. (13), (14), and (16) results in the following condition:

$$-\frac{\xi_{\text{sat}}^{90\%}}{\lambda_p} > 0.27 N_{\text{eff}}, \quad (17)$$

where  $N_{\text{eff}} = 2\tau_{\text{FWHM}}/T_p$  is defined as the effective number of pulses in the pulse train. Substituting this expression along with Eq. (16) into Eq. (14) yields the resonant detuning limit for wake fields driven by P-MoPA pulse trains:

$$\phi_{\text{max}}^{90\%} = \frac{E_{\text{max}}^{90\%}}{E_{\text{wb}}} < \frac{2.8}{\sqrt{N_{\text{eff}}}}. \quad (18)$$

For example, for  $\tau_{\text{FWHM}} = 2$  ps at  $n_{00} = 2.5 \times 10^{17} \text{ cm}^{-3}$ , a P-MoPA would form a pulse train comprised of  $N_{\text{eff}} = 18$  pulses. Substituting this into Eq. (18) then limits the maximum accelerating gradient before detuning to  $E_{\text{max}} < 32 \text{ GV/m}$ , or  $< 66\%$  of the cold wave-breaking field. If we operate the P-MoPA in the linear and quasilinear regime, for which  $\phi_{\text{max}}^{90\%} \lesssim 0.5$ , then Eq. (18) becomes  $N_{\text{eff}} < 30$ . We therefore conclude that wakefield saturation caused by this detuning mechanism will not be an issue for a drive train comprising  $\sim 30$  or fewer pulses.

A further consideration for P-MoPA pulse trains is that the individual pulses can be much shorter than in PBWA, such that  $a \ll 1$  can no longer be assumed. Thus, to maximize the wake amplitude, the relativistic effects associated with the quiver motion in regions of high intensity, rather than the relativistic effects associated with the fluid motion, should also be corrected for by using a slightly higher plasma density in the accelerator than the modulator stage to counteract this detuning mechanism.

Aside from limiting the wakefield amplitude, resonant detuning can also lead to focusing and defocusing effects caused

by pulses copropagating with high amplitude regions of the wakefield. These effects are discussed in the next section.

## VI. RELATIVISTIC SELF-PHASE MODULATION AND TRANSVERSE MODE EXCITATION

Until now, we have been treating the pulse train envelope as unchanging as it propagates along the accelerator. While this assumption is useful for deriving scaling laws and isolating certain physics, in reality the pulse train is a dynamic 3D structure which will evolve under the influence of both relativistic nonlinearities and its own excited wake. Neglecting depletion for now, the two main effects to consider for MP-LWFA in long channels are relativistic self-phase modulation (SPM) and transverse mode dynamics caused by the excitation of higher order transverse channel modes by the focusing and defocusing effects of the large amplitude wake.

Relativistic SPM causes further red- and blueshifting near the head or tail of each pulse, especially for the shortest duration, highest  $a_0$  pulses. Transverse mode excitation results in spot size oscillations and hence oscillations in the wakefield structure, which become more pronounced towards the back of the pulse train where the wake amplitude is the greatest. These oscillations could negatively affect beam quality, since a propagation-varying focusing field could increase the energy spread and emittance of the accelerated bunch.

Before significant pump depletion has occurred, i.e., while the frequencies within the laser spectrum satisfy  $|\omega - \omega_L|/\omega_L \ll 1$ , the evolution of the pulse train propagating in an axisymmetric channel of the form  $n_0(r) = n_{00} + \delta n_0(r)$  can be described using the paraxial wave equation in the weakly relativistic limit [34–37]

$$\left[ \frac{i}{\omega_L} \frac{\partial}{\partial \tau} + \frac{c^2}{2\omega_L^2} \Delta_{\perp} \right] a = \frac{\omega_p^2}{2\omega_L^2 n_0} [\delta n_0(r) + \delta n(r, \xi; |a|^2) - n_0(r)|a|^2/4] a, \quad (19)$$

where  $a(r, \theta, \xi, \tau)$  is the envelope of the normalized vector potential of the pulse,  $\omega_L$  is the laser frequency, and the propagation is described in comoving coordinates  $\xi = z - v_{g0}t$ ,  $\tau = t$ , with  $v_{g0}/c = (1 - \omega_{p0}^2/\omega_L^2)^{1/2}$  defined as the group velocity of electromagnetic plane waves in uniform plasma of density  $n_{00}$ , corresponding to the on-axis plasma channel frequency  $\omega_{p0}$ , and  $\Delta_{\perp} = \partial^2/\partial r^2 + (1/r)\partial/\partial r + (1/r^2)\partial^2/\partial \theta^2$  is the transverse Laplacian. Preformed plasma channels have often been modeled using parabolic transverse profiles, since these guide Laguerre-Gaussian modes. The long ( $\gtrsim 100$  mm), low-attenuation, and kHz production rate plasma channels required for this scheme have been experimentally demonstrated using the CHOFI technique [29–31], which forms deep, low-loss channels with on-axis densities as low as  $1 \times 10^{17} \text{ cm}^{-3}$ . These CHOFI channels are often better modelled with transverse profiles closer to square rather than parabolic [30], meaning that wake phase-front curvature effects can be neglected. In the following analysis, we will use a simplified profile and treat the plasma channel as an infinite square well of the form

$$n_0(r) = \begin{cases} n_{00} & r \leq R_{\infty} \\ \infty & r > R_{\infty}, \end{cases} \quad (20)$$

where  $R_{\infty}$  indicates the wall radius parameter specifically for this infinite square well. Note that the analysis that follows can be generalized to any axisymmetric, monotonically increasing channel profile. Assuming that the channel is unperturbed and that relativistic effects are negligible, substituting Eq. (20) into Eq. (19) yields the following orthogonal set of Bessel mode solutions for  $r \leq R_{\infty}$ :

$$a_{pm}(r, \theta, \xi, \tau) = \alpha_{pm}(\xi) \mathcal{J}_{pm}(r, \theta) e^{-i\Omega_{pm}\tau},$$

$$\mathcal{J}_{pm}(r, \theta) = \frac{J_1(j_{0,1})}{|J_{|m|+1}(j_{|m|,p+1})|} J_{|m|} \left( j_{|m|,p+1} \frac{r}{R_{\infty}} \right) e^{im\theta},$$

$$\Omega_{pm} = \frac{j_{|m|,p+1}^2 c^2}{2\omega_L R_{\infty}^2}, \quad (21)$$

where the integers  $p \geq 0$  and  $m$  are the radial and azimuthal indexes, respectively. Note that the effective spot size  $w_{0,\text{eff}}$  of the fundamental mode is related to the wall radius  $R_{\infty}$  by

$$w_{0,\text{eff}} = \sqrt{\frac{\int_0^R 2r^2 \mathcal{J}_{00}^2(r) r dr}{\int_0^R \mathcal{J}_{00}^2(r) r dr}} \approx 0.66 R_{\infty}, \quad (22)$$

which is analogous to the result for the standard step-index waveguide in the limit of infinite  $V$  number [38]. Similar to a previous analysis of the P-MoPA modulator stage [17], long-propagation of pulse trains in plasma channels are expected to excite higher order transverse channel modes, with an amplitude that scales with the wake amplitude. To model this effect, we first assume a fixed multipulse-driven wake of the form

$$\delta n(r, \xi) = \delta n_a(\xi) \mathcal{J}_{00}^2(r), \quad (23)$$

which is consistent with a pulse train primarily in the fundamental mode exciting a wake in the (quasi)linear regime. Applying time-dependent perturbation theory (TDPT) to Eq. (19) for pulses propagating in a square channel with only the  $m = 0$  radial transverse modes present, we find the following set of PDEs for the coefficients  $\alpha_p(\xi, \tau)$  of each of the square channel's radial modes  $\mathcal{J}_{p0}(r)$ :

$$i \frac{\partial \alpha_p(\xi, \tau)}{\partial \tau} = \frac{\omega_{p0}^2}{2\omega_L} \sum_n \alpha_n(\xi, \tau) \langle \mathcal{J}_{p0} | \frac{\delta n}{n_{00}} - \frac{|a|^2}{4} | \mathcal{J}_{n0} \rangle$$

$$\times e^{i(\Omega_{p0} - \Omega_{n0})\tau},$$

$$a(r, \xi, \tau) = \sum_p \alpha_p(\xi, \tau) \mathcal{J}_{p0}(r) e^{-i\Omega_{p0}\tau},$$

$$\langle \mathcal{J}_{p'm'} | (\dots) | \mathcal{J}_{pm} \rangle \equiv \frac{\int_0^{2\pi} d\theta \int_0^R r dr \mathcal{J}_{p'm'}^*(\dots) \mathcal{J}_{pm}}{J_1^2(j_{0,1}) \pi R_{\infty}^2}. \quad (24)$$

We note that TDPT requires that  $\pi r_e (2R_{\infty}/j_{0,1})^2 \delta n \ll 1$ , which is *not* true everywhere in the accelerator stage due to the large amplitude wake. However, for a resonant pulse train, the zeros of  $\delta n_a(\xi)$  are located near the laser centroids, so TDPT is still valid provided that the duration of each pulse is short, so  $\delta n$  is sufficiently small in regions of high intensity. Hence, we can still use TDPT to describe the evolution of the pulse train despite the large amplitude wake.

Assuming that most of the light is initially in the fundamental mode, transverse mode transitions will be dominated

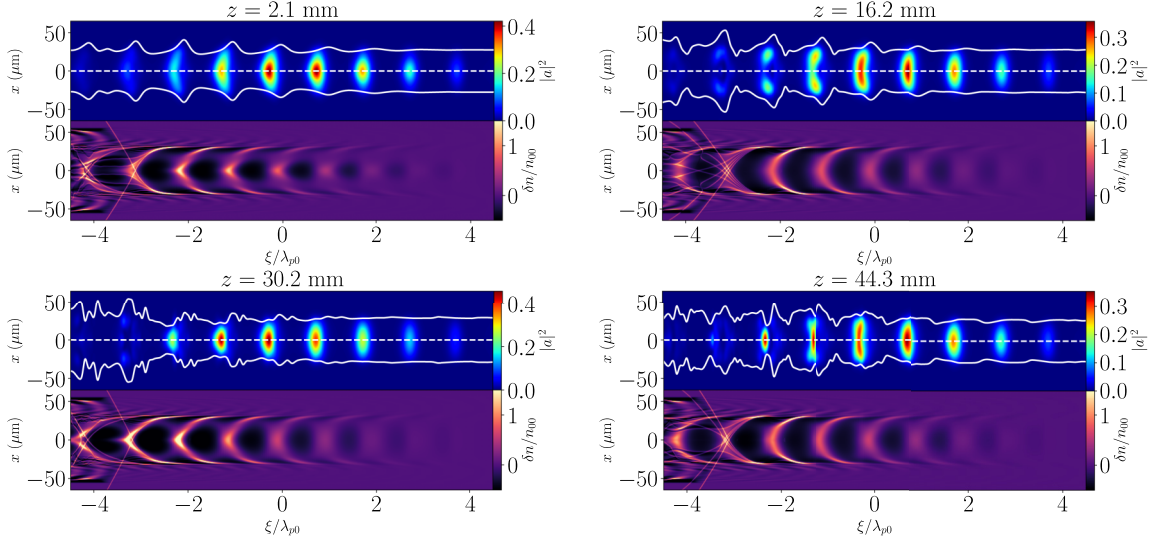


FIG. 3. Results of a 2D PIC simulation of the propagation of a pulse train in a quasi-square plasma channel. For this simulation,  $\xi$  as defined after Eq. (19) at varying propagation distances  $z$  in a quasi-square channel of the form given in Eq. (7) with  $n_{00} = 2.5 \times 10^{17} \text{ cm}^{-3}$ ,  $\Delta n = 1.26 \times 10^{17} \text{ cm}^{-3}$ ,  $R = 30 \text{ } \mu\text{m}$ ,  $W_{\text{drive}} = 2.4 \text{ J}$ ,  $\tau_{\text{drive}} = 1 \text{ ps}$  and modulator parameter  $\beta = 1.2$ . The pulse train at the entrance of the channel initially has a Gaussian transverse profile with spot size  $w_0 = 30 \text{ } \mu\text{m}$ . For each plot, the top panel displays the laser intensity profile  $|a|^2$  along with the local longitudinal variation of the laser centroid  $x_c(\xi)$  (dashed) and local effective spot size  $w_{\text{eff}}(\xi)$  (solid). The bottom panel displays the wake density perturbation  $\delta n/n_{00}$ .

by excitations of only the first radial mode, with higher order mode excitations being much weaker. Hence substituting our expression for the wake and approximating Eq. (24) as a two-level system description of the fundamental and first radial transverse modes yields

$$\begin{aligned} \frac{\partial}{\partial \tau} \begin{pmatrix} \alpha_0 \\ \alpha_1 \end{pmatrix} &= \mathbf{D}(\xi, \tau) \begin{pmatrix} \alpha_0 \\ \alpha_1 \end{pmatrix}, \\ \mathbf{D}(\xi, \tau) &= -i\gamma(\xi) \begin{pmatrix} d_{00} & d_{01} e^{-i\omega_w \tau} \\ \text{c.c.} & d_{11} \end{pmatrix}, \\ \gamma(\xi) &= \frac{\omega_{p0}^2}{2\omega_L} \left( \frac{\delta n_a(\xi)}{n_{00}} - \frac{|a_0|^2 f_{\text{acc}}^2(\xi)}{4} \right), \\ \omega_w &= \Omega_{10} - \Omega_{00} \approx \frac{12.3 c^2}{\omega_L R_\infty^2}, \\ d_{00} &= \langle \mathcal{J}_{00} | \mathcal{J}_{00}^2 | \mathcal{J}_{00} \rangle \approx 0.57 \\ d_{01} &= \langle \mathcal{J}_{00} | \mathcal{J}_{00}^2 | \mathcal{J}_{10} \rangle \approx 0.27, \\ d_{11} &= \langle \mathcal{J}_{10} | \mathcal{J}_{00}^2 | \mathcal{J}_{10} \rangle \approx 0.48, \end{aligned} \quad (25)$$

where  $\omega_w$  is the spot-size oscillation frequency, c.c. indicates the complex conjugate of the upper antidiagonal entry, and we have assumed the fundamental intensity profile  $|a|^2 \approx |a_0|^2 f_{\text{acc}}^2(\xi) \mathcal{J}_{00}^2(r)$  for the weakly relativistic term. This linear system of PDEs can then be solved analytically:

$$\begin{aligned} \begin{pmatrix} \alpha_0(\xi, \tau) \\ \alpha_1(\xi, \tau) \end{pmatrix} &= \mathbf{A}(\xi, \tau) \begin{pmatrix} \alpha_0(\xi, 0) \\ \alpha_1(\xi, 0) \end{pmatrix}, \\ \mathbf{A}(\xi, \tau) &= \exp \left[ -i\gamma(\xi) \tau \begin{pmatrix} d_{00} & d_{01} \text{sinc}(\frac{\omega_w \tau}{2}) e^{-i\omega_w \tau/2} \\ \text{c.c.} & d_{11} \end{pmatrix} \right], \\ w_{\text{eff}}(\xi, \tau) &\approx w_{0,\text{eff}} \left( 1 - 0.40 \frac{\alpha_0^* \alpha_1 e^{-i\omega_w \tau} + \text{c.c.}}{|\alpha_0|^2} \right). \end{aligned} \quad (26)$$

This solution describes the excitation of the first radial transverse mode due to transverse (de)focusing and self-modulation, both of which can arise through the effects of the wake and self-focusing. The interference between the fundamental and first radial mode then leads to a modulation of the local effective spot size  $w_{\text{eff}}(\xi, \tau)$ . Evaluating this matrix exponential yields a unitary matrix with diagonal entries of  $O(1)$  and antidiagonal entries of  $O(\gamma/\omega_w) \ll 1$ . This ensures that, as long as the original TDPT condition is satisfied in regions of high intensity, laser light initially in the fundamental transverse channel mode will also remain primarily in the fundamental mode, with small  $O(\gamma^2/\omega_w^2)$  and  $O(|\delta w|^2/w_0^2)$  oscillating exchanges in energy between the fundamental and first radial modes, where  $\delta w/w_0 \ll 1$  is some small initial spot size mismatch.

Since the bulk of the wake is already excited by the zeroth order intensity  $\sim \mathcal{J}_{00}^2(r)$ , we can neglect the wake contribution of the  $O(\gamma/\omega_w) \ll 1$ ,  $\sim \mathcal{J}_{00}(r) \mathcal{J}_{10}(r)$  first-order correction to the laser transverse mode dynamics. However, the near-axis wakefield itself can be significantly affected as laser energy continuously oscillates towards and away from the axis, resulting in propagation-dependent accelerating and focusing fields which could, in principle, impact both the emittance and energy spread of an injected electron bunch.

An example of this phenomenon in 2D PIC simulations is evident in Fig. 3, which shows snapshots of the laser intensity envelope and density perturbation as it propagates in a quasi-square channel. We can see that transverse mode excitation is the strongest for the trailing pulses which copropagate with the largest amplitude wake, as described by Eq. (26). This results in an oscillation of the wake structure and hence the maximum on-axis accelerating field  $E_{\text{max}}$ . (This oscillation of on-axis field can also be observed directly in Fig. 5, as we discuss below.) Despite the transverse mode excitation

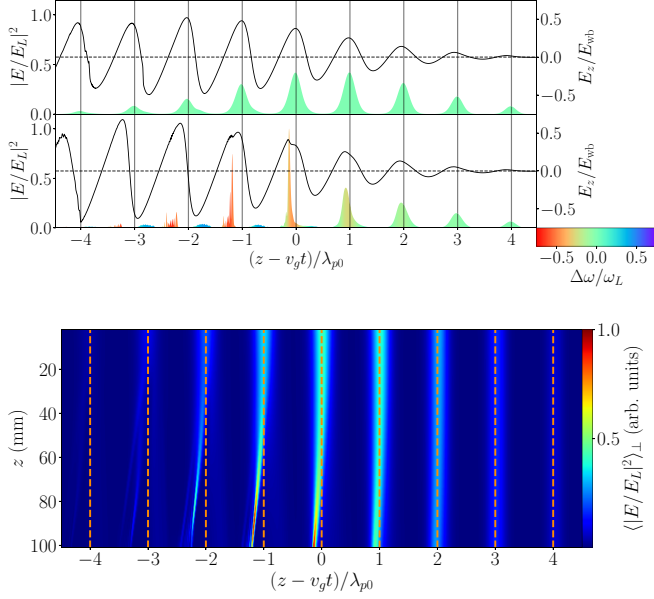


FIG. 4. Results from the same PIC simulation presented in Fig. 3. (a) The on-axis normalized axial electric field  $E_z/E_{wb}$  (solid, black) and the normalized laser intensity envelope  $|E/E_L|^2$  with  $E_L = m_e \omega_L c/e$  and its shift in instantaneous frequency  $\Delta\omega/\omega_L$  (color scale) after 2 mm (top) and 100 mm (bottom) of propagation. (b) The evolution of the transverse-averaged intensity envelope  $\langle |E/E_L|^2 \rangle_{\perp}$ . Note that  $|E/E_L| \neq |a|$  at large propagation distances due to the significant red-shifting of the trailing pulses.

causing a breakup of the trailing pulses, Figs. 3 and 4 show that the pulse train is still able to resonantly excite a wakefield even in the quasilinear regime with  $E_{\max}/E_{wb} \sim 0.5$ .

To compare the spot-size oscillation frequency  $\omega_w$  for a square channel given in Eq. (25) with the PIC simulations presented in Fig. 5, a correction has to be made for the fact that the plasma channel used in all of the presented PIC simulations is quasisquare with walls of finite height and width of the form given in Eq. (7). For this quasisquare channel, we define an effective channel radius,  $R_{\infty}^{\text{eff}}$ , as that radius for which the fundamental mode,  $\mathcal{J}_{00}(r)$ , of an infinite square channel best matches the lowest-order mode of the quasisquare channel. For the  $R = 30 \mu\text{m}$  case, this results in an effective channel radius of approximately  $R_{\infty}^{\text{eff}} \approx 46 \mu\text{m}$ . Substituting this into Eq. (25) then gives a spot-size oscillation wavelength of  $2\pi c/\omega_w \approx 6.6 \text{ mm}$ , which is in good agreement with the observed oscillation period of the on-axis accelerating field in Figs. 5(a) and 5(b).

Various strategies can be employed to minimize this effect. First, and most obviously, the mode of the input pulse train should be matched to the lowest-order mode of the channel as closely as possible, which would minimize oscillations associated with  $|\delta w|/w_0$ . Next, the following quantity, which is a measure of the oscillation of the wakefield structure behind the pulse train, should be minimized:  $|(\int_{-\infty}^{\infty} d\xi (\gamma(\xi)/\omega_w) f_{\text{acc}}^2(\xi)) / (\int_{-\infty}^{\infty} d\xi f_{\text{acc}}^2(\xi))|$ . For a given wake amplitude  $\delta n_a(\xi)/n_{00}$ , the two ways to minimize this quantity are (i) to reduce detuning effects to ensure that the plasma wave zeros are as close to the pulse centroids as possible and (ii) to increase the modulator parameter  $\beta$ , which

shortens the duration of each pulse in the train, so they only sample the plasma wave close to its zero crossings; although we note that this latter strategy also increases SPM, which hastens the onset of depletion effects towards the heads of the pulses.

We also note that propagation over long distances in a finite plasma channel damps spot-size oscillations by preferentially leaking out higher-order modes [39]. This, in combination with the spot-size oscillation frequency locally varying across each single pulse due to  $\gamma(\xi)$ , causes the on-axis accelerating field to stabilize after some distance, as observed in Fig. 5.

## VII. DEPLETION EFFECTS

We also have to consider that the paraxial description which led to the result in Eq. (26) breaks down when depletion becomes non-negligible, which becomes important when driving quasilinear wakes where the dephasing length is a large fraction of the depletion length.

One caveat to the earlier analysis of the depletion length in Eq. (6) is that pulse trains do not deplete uniformly. Instead, trailing pulses, which copropagate with steeper density gradients, will deplete faster than those near the beginning of the pulse train. We thus expect the pulses towards the rear of the train to have individual depletion lengths up to half as short as in Eq. (6), while the pulses near the beginning of the train will experience minimal depletion.

The nonuniform depletion effects include group velocity dispersion between the pulses, caused by the trailing depleted pulses slowing down more, and detuning spot size oscillations as depleted pulses have shorter spot size oscillation periods due to their shorter Rayleigh lengths.

As demonstrated in Fig. 4, the pulse train is initially uniformly spaced and can therefore suffer from Rosenbluth-Liu detuning, though it remains a small effect due to the low number of pulses. However, as the pulse train depletes, the strongly redshifting trailing pulses fall behind and become resonant with the wake. We also observe a small portion of the heads of each of the trailing pulses strongly blueshifting and catching up with the train.

The onset of depletion effects is also expedited by relativistic SPM, as this increases the rate at which the heads of each pulse in the pulse train red-shifts and causes pulse steepening [40], which is observed in Fig. 4(a). On one hand, depletion causes bunch dephasing to occur sooner than predicted by Eq. (3) by a reduction in group velocity. On the other hand, the resulting reduction in instantaneous laser frequency increases the ponderomotive force (which scales with  $F_p \propto \omega^{-1}$  when holding photon number density constant), causing the wakefield amplitude to gradually increase with propagation distance, similar to the effect observed experimentally by Streeter *et al.* [41].

## VIII. MULTI-GEV P-MOPA ELECTRON ACCELERATOR

Figure 5 summarizes the performance of the accelerator stage of a P-MoPA for several different drive lasers and modulator stage parameters. The parameters selected take into account the constraints set by the modulator stage (which



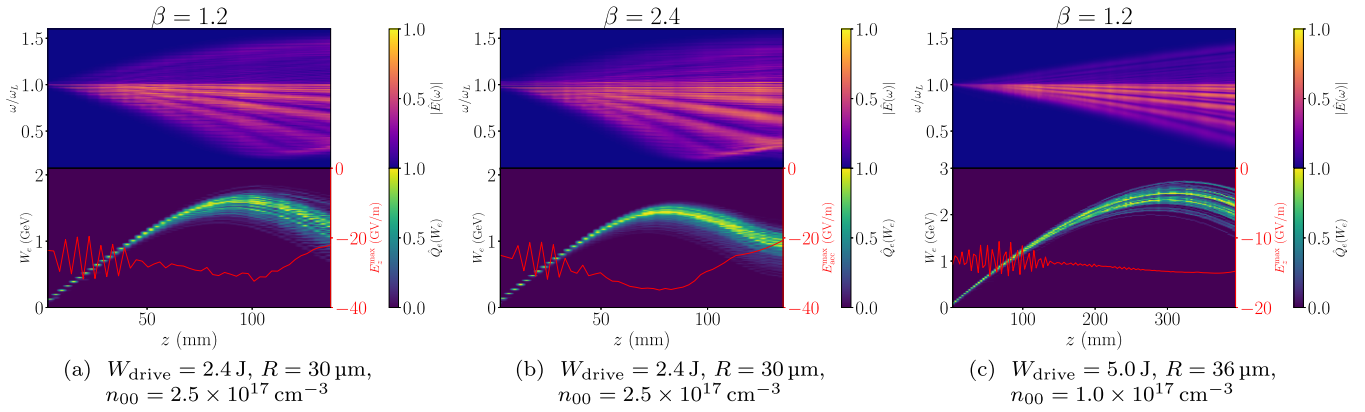


FIG. 5. 2D PIC simulation results of accelerator performance at different modulation parameters  $\beta$  in a quasisquare channel of the same form used in Fig. 3. The top panels display the normalized laser spectrum  $|\hat{E}(\omega)|$  evolving with the propagation distance, while the bottom panels show the evolution of the normalized injected bunch electron energy spectrum  $\hat{Q}_e(W_e)$  and maximum on-axis accelerating field  $E_{\text{acc}}^{\text{max}}$ . Note that the oscillation of the on-axis accelerating field due to spot-size oscillations is a continuous sinusoidal motion which disappears beyond 50 mm in (a), (b) and 130 mm in (c), and only appears to be jagged in these plots due to subsampling.

sets a limit on  $W_{\text{drive}}$  for a given modulator spot size and plasma density [17], relativistic detuning effects, optimizing the wake amplitude (by using a suitable modulator parameter  $\beta$ ) and the evolution with  $z$  of the wakefield (caused by SPM and transverse mode excitation). The figures show the evolution of the laser spectra, maximum on-axis accelerating wakefield, and the energy of a test electron bunch. For these 2D PIC simulations, a 1 pC, 35 MeV Gaussian electron bunch was manually placed in phase with the peak accelerating wakefield with dimensions  $x_{\text{rms}} = 4 \mu\text{m}$ ,  $z_{\text{rms}} = 1.5 \mu\text{m}$  for  $n_{00} = 2.5 \times 10^{17} \text{ cm}^{-3}$ . The bunch dimensions were scaled up by a factor of  $\sqrt{2.5}$  for the  $n_{00} = 1.0 \times 10^{17} \text{ cm}^{-3}$  simulation.

For  $n_{00} = 2.5 \times 10^{17} \text{ cm}^{-3}$ , the observed propagation distance at which the maximum energy gain is achieved for the  $\beta = 1.2$  case corresponds well with  $L_d = 93 \text{ mm}$  predicted by Eq. (3) using  $R_{\infty}^{\text{eff}} = 46 \mu\text{m} \Rightarrow w_{0,\text{eff}} = 30 \mu\text{m}$ . The laser-plasma energy transfer is found from the PIC simulations to be 16%. According to Eq. (3),  $L_d$  is independent of  $\beta$ , but Fig. 5(b) shows that increasing  $\beta$  to 2.4 causes  $L_d$  to decrease to 80 mm. The higher value of beta is also found to increase the laser-plasma energy transfer to 19%, primarily due to the earlier onset of pump depletion via SPM, as is evident by comparing the laser spectra in Figs. 5(a) and 5(b). Despite the earlier onset of pump depletion for the higher  $\beta$  case, the mean energy gain for both values of  $\beta$  is approximately  $\sim 1.5 \text{ GeV}$ . This value is in good agreement with Eq. (4), which predicts an energy gain of  $\Delta W_e = 1.4 \text{ GeV}$  for a relative wake amplitude of  $E_{\text{max}}/E_{\text{wb}} = 0.5$ , consistent with the amplitude observed in PIC simulation shown in Figure 4.

Figure 5(c) shows the result for a lower density accelerator stage with  $n_{00} = 1.0 \times 10^{17} \text{ cm}^{-3}$  and  $w_0 = 36 \mu\text{m}$  at  $\beta = 1.2$ . The evolution of the pulse train spectrum, accelerating field, and bunch energy is shown for lengths up to 400 mm. A bunch of energy around 2.5 GeV is obtained, which is in good agreement with the value of  $\Delta W_e = 2.6 \text{ GeV}$  given by Eq. (4) for  $E_{\text{max}}/E_{\text{wb}} = 0.46$  (which is slightly lower than the previous simulations due to the scaled laser energy density  $W_{\text{drive}}/w_0^2\lambda_{p0}$  being 8.5% smaller). Figure 5(c) shows that dephasing occurs at  $z = L_d = 300 \text{ mm}$ , which is close

to the value of 296 mm predicted from Eq. (3). It is clear from these simulations that P-MoPAs operating at multi-GeV energy gains should be possible.

All three simulations shown in Fig. 5 exhibit the expected oscillation in peak on-axis accelerating field due to transverse oscillations of the pulses in the train, as discussed in the previous section and observed in Fig. 3. In addition, Fig. 5 shows that the accelerating field initially grows in magnitude with propagation. This increase arises from (i) SPM-induced pulse steepening; (ii) the effect shown in Fig. 4, whereby greater red-shifting of the trailing pulses in the train causes the pulse separation to increase towards the back of the train, partially circumventing Rosenbluth-Liu detuning; and (iii) an increase in the ponderomotive force exerted by the trailing pulses, which arises from their greater redshift.

## IX. CONCLUSION

We have studied the operation of the accelerator stage in a P-MoPA using both the paraxial wave equation in the weakly relativistic limit and 2D PIC simulations.

The ability to adjust the modulator parameter  $\beta$  was found to bring several advantages. First, unlike in the PBWA, it allows the temporal envelope of pulses within the pulse train to be controlled. For the optimal value of  $\beta = 1.43$ , the wake amplitude was found to be 72% larger than that generated in a PBWA with the same total drive energy. Second, adjusting  $\beta$  can minimize transverse mode excitation, and hence oscillation of the wakefield structure, which is likely, in turn, to minimize increases in the energy spread and emittance of an injected electron bunch.

Rosenbluth-Liu detuning was found to be much less important in a P-MoPA than it is in a PBWA, for two reasons. First, our analysis shows that in the linear and quasilinear regimes, Rosenbluth-Liu detuning would not occur appreciably if the number of pulses in the P-MoPA train was less than  $\sim 30$ . Second, in a P-MoPA operating in the quasilinear regime, this detuning is at least partially counteracted by the increase in pulse spacing towards the back of the train caused by increased redshifting.

We presented an analysis of transverse mode oscillations within the paraxial approximation, which was found to be in good agreement with 2D PIC simulations. PIC simulations for several combinations of laser and plasma parameters showed good agreement with expressions derived for the spot-size oscillation frequency, pump depletion, dephasing length, and energy gain. These simulations demonstrate that particle energy gains of several GeV should be possible in a P-MoPA.

We note that in this paper we ignored the effects of the accelerated bunch on the wakefield. In addition to decreasing the acceleration gradient—which has the compensating advantage of providing a means to reduce the bunch energy spread—beamloading effects could introduce a coupling between the pulse train and the injected bunch dynamics. This will be a subject for future research.

The work presented in this paper confirms that P-MoPAs driven by few-joule, picosecond pulses, such as those provided by high-repetition-rate thin-disk lasers, have the potential to accelerate electron bunches to multi-GeV energies at pulse repetition rates in the kilohertz range.

## ACKNOWLEDGMENTS

This paper was supported by the UK Engineering and Physical Sciences Research Council (EPSRC) (Grant No. EP/V006797/1), the UK Science and Technologies Facilities Council (Grant No. ST/V001655/1), InnovateUK (Grant No. 10059294), United Kingdom Research and Innovation (UKRI) ARCHER2 Pioneer Projects (No. ARCHER2 PR17125) [42], and the Ken and Veronica Tregidgo Scholarship in Atomic and Laser Physics. This publication arises from research funded by the John Fell Oxford University Press Research Fund. This research used the open-source particle-in-cell code WARPX [18,43], primarily funded by the U.S. DOE Exascale Computing Project. Primary WARPX contributors are with LBNL, LLNL, CEA-LIDYL, SLAC, DESY, CERN, and Modern Electron. We acknowledge all WARPX contributors. This research was funded in whole, or in part, by EPSRC and STFC, which are Plan S funders. The input decks used for the PIC simulations presented in this paper are available at Ref. [44]

- 
- [1] T. Tajima and J. M. Dawson, Laser electron accelerator, *Phys. Rev. Lett.* **43**, 267 (1979).
  - [2] M. N. Rosenbluth and C. S. Liu, Excitation of plasma waves by two laser beams, *Phys. Rev. Lett.* **29**, 701 (1972).
  - [3] E. Esarey, A. Ting, and P. Sprangle, Relativistic focusing and beat wave phase velocity control in the plasma beat wave accelerator, *Appl. Phys. Lett.* **53**, 1266 (1988).
  - [4] P. Gibbon, The self-trapping of light waves by beat-wave excitation, *Phys. Fluids B: Plasma Phys.* **2**, 2196 (1990).
  - [5] S. Y. Tochitsky, R. Narang, C. V. Filip, P. Musumeci, C. E. Clayton, R. B. Yoder, K. A. Marsh, J. B. Rosenzweig, C. Pellegrini, and C. Joshi, Enhanced acceleration of injected electrons in a laser-beat-wave-induced plasma channel, *Phys. Rev. Lett.* **92**, 095004 (2004).
  - [6] S. M. Hooker, R. Bartolini, S. P. D. Mangles, A. Tünnemann, L. Corner, J. Limpert, A. Seryi, and R. Walczak, Multi-pulse laser wakefield acceleration: A new route to efficient, high-repetition-rate plasma accelerators and high flux radiation sources, *J. Phys. B: At. Mol. Opt. Phys.* **47**, 234003 (2014).
  - [7] D. Strickland and G. Mourou, Compression of amplified chirped optical pulses, *Opt. Commun.* **56**, 219 (1985).
  - [8] J. W. Dawson, J. K. Crane, M. J. Messerly, M. A. Prantil, P. H. Pax, A. K. Sridharan, G. S. Allen, D. R. Drachenberg, H. H. Phan, J. E. Heebner, C. A. Ebberts, R. J. Beach, E. P. Hartouni, C. W. Siders, T. M. Spinka, C. P. J. Barty, A. J. Bayramian, L. C. Haefner, F. Albert, W. H. Lowdermilk *et al.*, High average power lasers for future particle accelerators, *AIP Conf. Proc.* **1507**, 147 (2012).
  - [9] B. Hidding, S. Hooker, S. Jamison, B. Muratori, C. Murphy, Z. Najmudin, R. Pattathil, G. Sarri, M. Streecher, C. Welsch, M. Wing, and G. Xia, Plasma wakefield accelerator research 2019 - 2040: A community-driven UK roadmap compiled by the plasma wakefield accelerator steering committee (PWASC), [arXiv:1904.09205](https://arxiv.org/abs/1904.09205).
  - [10] O. Jakobsson, S. M. Hooker, and R. Walczak, GeV-scale accelerators driven by plasma-modulated pulses from kilohertz lasers, *Phys. Rev. Lett.* **127**, 184801 (2021).
  - [11] C. Herkommer, P. Krötz, R. Jung, S. Klingebiel, C. Wandt, R. Bessing, P. Walch, T. Produit, K. Michel, D. Bauer, R. Kienberger, and T. Metzger, Ultrafast thin-disk multipass amplifier with 720 mJ operating at kilohertz repetition rate for applications in atmospheric research, *Opt. Express* **28**, 30164 (2020).
  - [12] S. Nagel, B. Metzger, D. Bauer, J. Dominik, T. Gottwald, V. Kuhn, A. Killi, T. Dekorsy, and S.-S. Schad, Thin-disk laser system operating above 10 kW at near fundamental mode beam quality, *Opt. Lett.* **46**, 965 (2021).
  - [13] T. Produit, P. Walch, C. Herkommer, A. Mostajabi, M. Moret, U. Andral, A. Sunjerga, M. Azadifar, Y.-B. André, B. Mahieu, W. Haas, B. Esmiller, G. Fournier, P. Krötz, T. Metzger, K. Michel, A. Mysyrowicz, M. Rubinstein, F. Rachidi, J. Kasparian *et al.*, The laser lightning rod project, *Eur. Phys. J. Appl. Phys.* **93**, 10504 (2021).
  - [14] R. Paschotta, J. Aus der Au, G. Spühler, S. Erhard, A. Giesen, and U. Keller, Passive mode locking of thin-disk lasers: Effects of spatial hole burning, *Appl. Phys. B* **72**, 267 (2001).
  - [15] T. Südmeyer, C. Kränkel, C. Baer, O. Heckl, C. Saraceno, M. Golling, R. Peters, K. Petermann, G. Huber, and U. Keller, High-power ultrafast thin disk laser oscillators and their potential for sub-100-femtosecond pulse generation, *Appl. Phys. B* **97**, 281 (2009).
  - [16] C. R. E. Baer, C. Kränkel, C. J. Saraceno, O. H. Heckl, M. Golling, R. Peters, K. Petermann, T. Südmeyer, G. Huber, and U. Keller, Femtosecond thin-disk laser with 141 W of average power, *Opt. Lett.* **35**, 2302 (2010).
  - [17] J. J. van de Wetering, S. M. Hooker, and R. Walczak, Stability of the modulator in a plasma-modulated plasma accelerator, *Phys. Rev. E* **108**, 015204 (2023).
  - [18] L. Fedeli, A. Huebl, F. Boillod-Cerneux, T. Clark, K. Gott, C. Hillairet, S. Jaure, A. Leblanc, R. Lehe, A. Myers, C. Piechurski, M. Sato, N. Zaim, W. Zhang, J. Vay, and H. Vincenti, Pushing the frontier in the design of laser-based electron accelerators with groundbreaking mesh-refined particle-in-cell simulations on exascale-class supercomputers,

- in *2022 SC22: International Conference for High Performance Computing, Networking, Storage and Analysis (SC) (SC)* (IEEE Computer Society, Los Alamitos, CA, 2022), pp. 25–36.
- [19] E. Esarey, C. B. Schroeder, and W. P. Leemans, Physics of laser-driven plasma-based electron accelerators, *Rev. Mod. Phys.* **81**, 1229 (2009).
- [20] C. Kurtz and W. Streifer, Guided waves in inhomogeneous focusing media part I: Formulation, solution for quadratic inhomogeneity, *IEEE Trans. Microw. Theory Tech.* **17**, 11 (1969).
- [21] W. Firth, Propagation of laser beams through inhomogeneous media, *Opt. Commun.* **22**, 226 (1977).
- [22] E. Esarey and W. P. Leemans, Nonparaxial propagation of ultrashort laser pulses in plasma channels, *Phys. Rev. E* **59**, 1082 (1999).
- [23] J. D. Sadler, C. Arran, H. Li, and K. A. Flippo, Overcoming the dephasing limit in multiple-pulse laser wakefield acceleration, *Phys. Rev. Accel. Beams* **23**, 021303 (2020).
- [24] C. B. Schroeder, E. Esarey, C. G. R. Geddes, C. Benedetti, and W. P. Leemans, Physics considerations for laser-plasma linear colliders, *Phys. Rev. ST Accel. Beams* **13**, 101301 (2010).
- [25] W. K. H. Panofsky and W. A. Wenzel, Some considerations concerning the transverse deflection of charged particles in radio-frequency fields, *Rev. Sci. Instrum.* **27**, 967 (1956).
- [26] L. M. Gorbunov and V. I. Kirsanov, Excitation of plasma waves by an electromagnetic wave packet, *Zh. Eksp. Teor. Fiz.* **93**, 509 (1987) [*Sov. Phys. JETP* **66**, 290 (1987)].
- [27] N. Andreev, E. Chizhonkov, A. Frolov, and L. Gorbunov, On laser wakefield acceleration in plasma channels, *Nucl. Instrum. Methods Phys. Res. Sect. A* **410**, 469 (1998).
- [28] A. von Boetticher, R. Walczak, and S. M. Hooker, Modulational instability in large-amplitude linear laser wakefields, *Phys. Rev. E* **107**, L023201 (2023).
- [29] A. Picksley, A. Alejo, R. J. Shalloo, C. Arran, A. von Boetticher, L. Corner, J. A. Holloway, J. Jonnerby, O. Jakobsson, C. Thornton, R. Walczak, and S. M. Hooker, Meter-scale conditioned hydrodynamic optical-field-ionized plasma channels, *Phys. Rev. E* **102**, 053201 (2020).
- [30] L. Feder, B. Miao, J. E. Shrock, A. Goffin, and H. M. Milchberg, Self-waveguiding of relativistic laser pulses in neutral gas channels, *Phys. Rev. Res.* **2**, 043173 (2020).
- [31] B. Miao, L. Feder, J. E. Shrock, A. Goffin, and H. M. Milchberg, Optical guiding in meter-scale plasma waveguides, *Phys. Rev. Lett.* **125**, 074801 (2020).
- [32] G. N. Watson, *A Treatise on the Theory of Bessel Functions*, 2nd ed. (Cambridge University Press, London, 1966).
- [33] I. S. Gradshteyn and I. M. Ryzhik, *Table of Integrals, Series, and Products*, 7th ed., translated from Russian, translation edited and with a preface by A. Jeffrey and D. Zwillinger (Elsevier/Academic Press, Amsterdam, 2007), pp. xlviii+1171.
- [34] E. Esarey, P. Sprangle, J. Krall, A. Ting, and G. Joyce, Optically guided laser wakefield acceleration, *Phys. Fluids B: Plasma Phys.* **5**, 2690 (1993).
- [35] N. E. Andreev, L. M. Gorbunov, V. I. Kirsanov, A. A. Pogosova, and R. R. Ramazashvili, The theory of laser self-resonant wake field excitation, *Phys. Scr.* **49**, 101 (1994).
- [36] P. Mora and T. M. Antonsen Jr., Kinetic modeling of intense, short laser pulses propagating in tenuous plasmas, *Phys. Plasmas* **4**, 217 (1997).
- [37] W. Zhu, J. P. Palastro, and T. M. Antonsen, Studies of spectral modification and limitations of the modified paraxial equation in laser wakefield simulations, *Phys. Plasmas* **19**, 033105 (2012).
- [38] E. Brinkmeyer, Spot size of graded-index single-mode fibers: Profile-independent representation and new determination method, *Appl. Opt.* **18**, 932 (1979).
- [39] B. Z. Djordjević, C. Benedetti, C. B. Schroeder, E. Esarey, and W. P. Leemans, Filtering higher-order laser modes using leaky plasma channels, *Phys. Plasmas* **25**, 013103 (2018).
- [40] W. Mori, The physics of the nonlinear optics of plasmas at relativistic intensities for short-pulse lasers, *IEEE J. Quantum Electron.* **33**, 1942 (1997).
- [41] M. J. V. Streeter, S. Kneip, M. S. Bloom, R. A. Bendoyro, O. Chekhlov, A. E. Dangor, A. Döpp, C. J. Hooker, J. Holloway, J. Jiang, N. C. Lopes, H. Nakamura, P. A. Norreys, C. A. J. Palmer, P. P. Rajeev, J. Schreiber, D. R. Symes, M. Wing, S. P. D. Mangles, and Z. Najmudin, Observation of laser power amplification in a self-injecting laser wakefield accelerator, *Phys. Rev. Lett.* **120**, 254801 (2018).
- [42] <https://www.archer2.ac.uk>.
- [43] <https://github.com/ECP-WarpX/WarpX>.
- [44] <https://doi.org/10.5281/zenodo.10061009>.